# A Correlation Between Seismic Tomography, Seismic Events and Support Pressure

E.C. Westman
*Department of Mining and Minerals Engineering, Virginia Tech, Blacksburg, Virginia, USA*
K.A. Heasley
*National Institute of Occupational Safety and Health, Pittsburgh, Pennsylvania, USA*
P.L. Swanson
*National Institute of Occupational Safety and Health, Spokane, Washington, USA*
S. Peterson
*RAG American Coal Corporation, USA*

ABSTRACT: Coal bumps are brittle, violent failures associated with high stresses and competent host strata. To study bump mechanisms, conditions in the vicinity of a deep longwall mining face in bump-prone strata were monitored using three discrete systems. First, a microseismic monitoring network recorded mining-induced seismic events throughout the mine and surrounding strata. Second, pressure variations and distributions on the longwall shield legs across the face were recorded. Last, tomography surveys imaged seismic transmission properties ahead of the face. Results from the three systems were correlated in an effort to increase understanding of mining-induced stress redistribution and bump potential. An initial, one-week study showed that the correlation between averaged tomogram values and seismically active areas had a coefficient of correlation (R) of 0.89. Further results of these studies demonstrate that the tomography system is capable of imaging heavy shield-leg loading and bump-prone conditions prior to them disrupting the face operations.

## INTRODUCTION

### *The Mine*

A modern longwall coal mine is a highly mechanized, capital intensive, system, typically producing more than 10,000 tonnes of coal per day with as few as 10 to 15 people operating the face equipment. Any capital-intensive operation must be continuously utilized to optimize the investment. Further, the profit margin for a longwall face is typically five times that of a room and pillar face. Any loss in production time, therefore, quickly translates into lost profits for the mine. Coal bumps, comparable to rock bursts in non-coal mines, are localized seismic events which can rapidly and forcefully eject many tons of coal into the mine openings. These events not only disrupt the mining process, they can also be extremely dangerous to underground personnel.

The longwall coal mine at which the monitoring occurred is located in the western United States. The seam is under approximately 800 m of massive competent overburden with a history of mining-related seismicity. Three systems were used to monitor the ground conditions at this underground longwall mine: a microseismic monitoring network, a seismic tomography system and a longwall shield-leg pressure recording system. Results from the monitoring systems were correlated in an effort to determine whether the diverse information could be used synergistically to increase understanding of mining-induced stress redistribution and bump potential.

### *Bumps*

Kusznir & Farmer (1983) defined a coal bump as a brittle failure associated with high stresses and strong rocks. Coal bumps have resulted in numerous fatalities historically, and continue to cause fatal accidents. In addition to the health and safety concerns, economic losses due to lost production are typically tens of thousands of dollars per day that a longwall face is inactive. Numerous factors have been stated to influence the occurrence of bumps, including properties of the coal, geology (joints, folds, faults, etc.), mining induced stresses, strong sandstone beds in the roof, pillar size and shape, mining technique, and mining rate (Holland 1958, Whittaker 1983, Iannacchione et al. 1987, Arabasz et al. 1997). Haramy & McDonnell (1988) emphasized that the energy released in a bump is from accumulated strain energy in the coal, roof, or floor. Strain energy accumulates in the strata as a result of deflection under abutment stresses. The roof strata deflect either by bridging or cantilevering. Failure of the coal is

termed a “pressure” bump, while failure of the roof is termed a “shock” bump (Mark et al. 1999).

### *Microseismic Monitoring Network*

Mine-scale seismic networks have been used for more than 30 years to monitor location and magnitude of mining-induced seismicity (Mendicki 1997). Young (1992) reported results of a study which correlated mining-induced seismicity and tomography at underground hardrock mines. The relationship between rock bursts, geology, and mine layout at an underground silver mine was described by Swanson (1995). Wilson & Kneisley (1995) discussed the results of studies monitoring mining-induced seismicity at four underground coal sites identifying potential trends leading to a high risk for bump events. The mine and the microseismic monitoring network used in this study are more completely described in Ellenberger et al. (2001).

### *Longwall Shields*

The roof above a longwall face is supported by numerous longwall shields. Each shield is typically between 1.5 and 2 meters wide and essentially consists of a base unit, hydraulic cylinders and a canopy. The hydraulic cylinders (or legs) press the canopy of the shield against the roof and control the roof stability above the working area. Modern shields can support up to 1000 tonnes of roof load. Hanna et al. (1991) and Cox et al. (1995) report on a system for monitoring roof stability conditions at a longwall face by recording the fluid pressure in the shield legs. Average leg pressures are reported and display loading trends which can be attributed to changing geologic and stress conditions at the face.

### *Tomography*

Tomographic imaging was first described by Radon (1917) who theorized that the interior of a body could be imaged by analyzing energy which passed from one boundary to another. This technology was eventually adapted to the medical field (Hounsfield 1973, Cormack 1973) and to the geosciences (Dines & Lytle 1979). Tomography has been used in the mining industry for at least 20 years to image geologic features as well as stress-related features (Buchanan et al. 1981, Mason 1981, Kormendi et al. 1986). More recently, the method has been adapted to image stress concentrations ahead of a longwall face by a unique application of the longwall mining equipment as the seismic source (Westman et al. 1996).

## METHODS AND PROCEDURES

In this paper, two data sets were analyzed, the first consisted of seismic events and tomograms from one week, representing approximately 90 m of face advance. Analysis of the first data set was completed during an on-site visit. Subsequently, a more comprehensive analysis was completed with a second data set. The second data set consisted of seismic events, shield leg pressures, and tomograms from a six-week time interval, representing approximately 240 m of face advance. The data manipulation and analysis process was essentially the same for the two data sets and will be described in the following sections.

### *Seismic System*

A three-dimensional, full-waveform, seismic network with both surface and underground sensors was established around the active mining panels. The purpose of the array was to determine the timing, exact location, magnitude, and mechanism (shear fracture, bedding plane slip, etc.) of the failure of the strata surrounding the mined panels. At the time of the study described in this paper, the underground array consisted of 13 geophones located about every 300 to 450 m around the active panel. The surface seismic array consisted of nine geophones strategically located above the longwall panel. In the final seismic dataset, only the events with a minimum of 8 total stations (with at least 3 surface stations and 3 underground stations) reporting good first-arrival picks were kept in the database. Figure 1 shows the location of the surface and underground geophones, as well as the location of the longwall face during acquisition of the two data sets.

Arabasz et al. (1997) reported that mining seismicity is well correlated to the rate of advance of the mining face. An comparison between the seismicity rate and face advance rate was performed for all seismic events within 60 m of the face and is presented in Figure 2 which clearly shows a strong correlation between rate of face advance and level of seismic activity. For correlating the seismic data with the shield leg pressures and the tomography output, the density of the seismicity was determined on a 7.5 by 7.5 m grid by calculating the number of events occurring per unit area in the plane of the seam.

### Shield Legs

Shield leg pressure data were gathered by using pressure transducers attached to the legs of each longwall shield. The transducers monitored the hydraulic pressure in the shield legs at five- to eight-

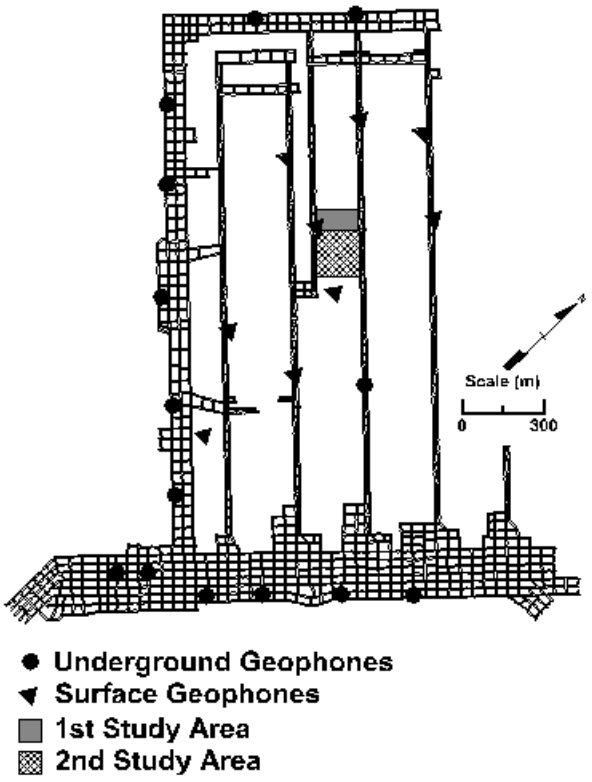


Figure 1. Location of surface (triangle) and underground (circle) seismic sensors and face locations during acquisition of two data sets.

minute intervals. These data were then reduced by averaging to create a grid with 7.5m cell sizes so that all the shield leg pressures as the face advanced over 7.5 m were averaged and adjacent shields were additionally averaged to create a pressure value for each 7.5 by 7.5-m cell.

*Tomography*

Mine personnel generated three to four tomograms each day. The longwall shearer was used as the source of seismic energy and geophones mounted on roofbolts in the headgate and tailgate were the receivers. Because the receivers were mounted on roofbolts, the tomograms are representative of conditions in the strata above the coal seam. For this analysis the tomograms were reduced to their raw transmission values broken into 7.5 by 7.5 m grids. Average tomograms were then calculated. This averaging results in a reduction in the visibility of stress-related features; however, the clarity of geologic anomalies, which are stationary in their location, is emphasized. Therefore, the average tomograms are expected to display geologic features across the panel, especially in the roof. The average tomograms were calculated in 7.5 m grids to allow correlation with the other monitored data.

## RESULTS

*One-Week Data Set*

Data collected as the face advanced 90 m during a one-week period in February, 2000 were analyzed initially. The goal of the analysis was to determine whether similar trends were present within both the seismic data set and the averaged tomograms. To accomplish this goal, the average transmission levels for the tomograms were summed for all cells at a given distance along the tailgate (in 7.5 m strips parallel to the longwall face). These results are shown

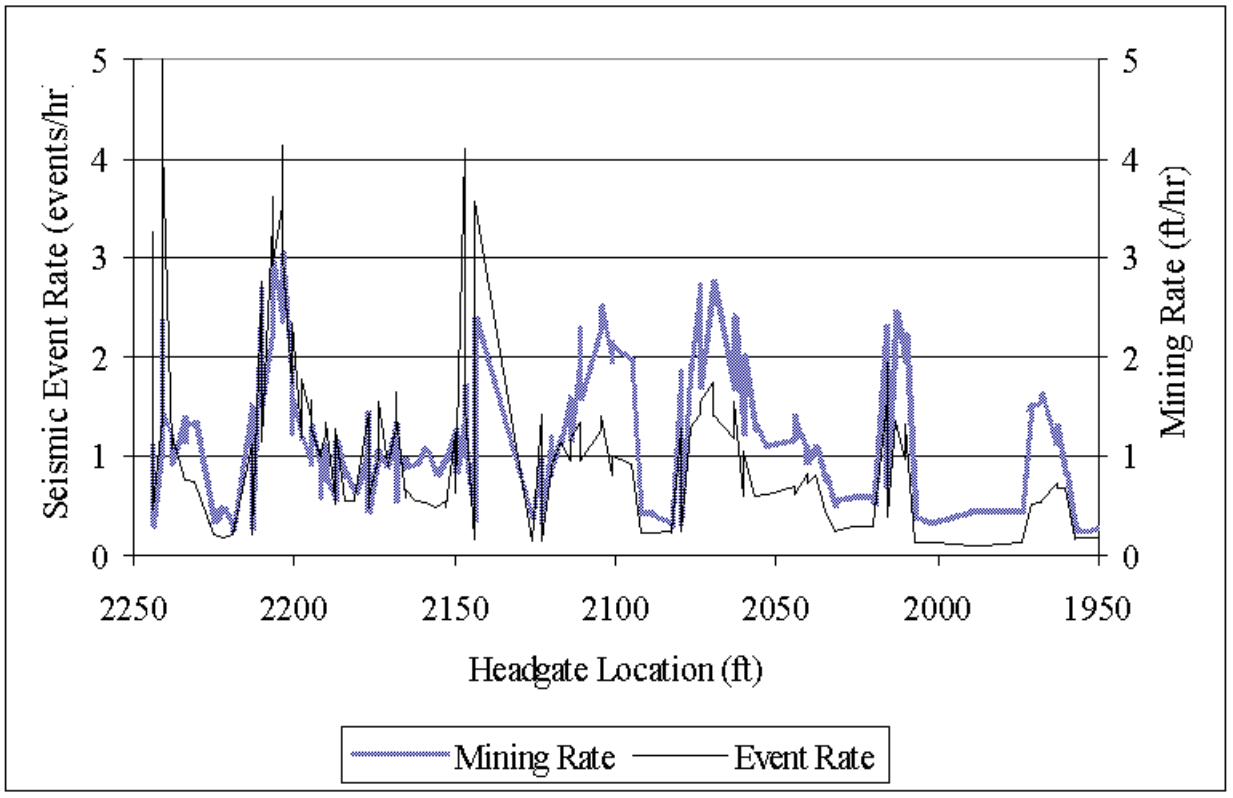


Figure 2. Mining rate and seismic event rate, for time period of February 14-21, 2000

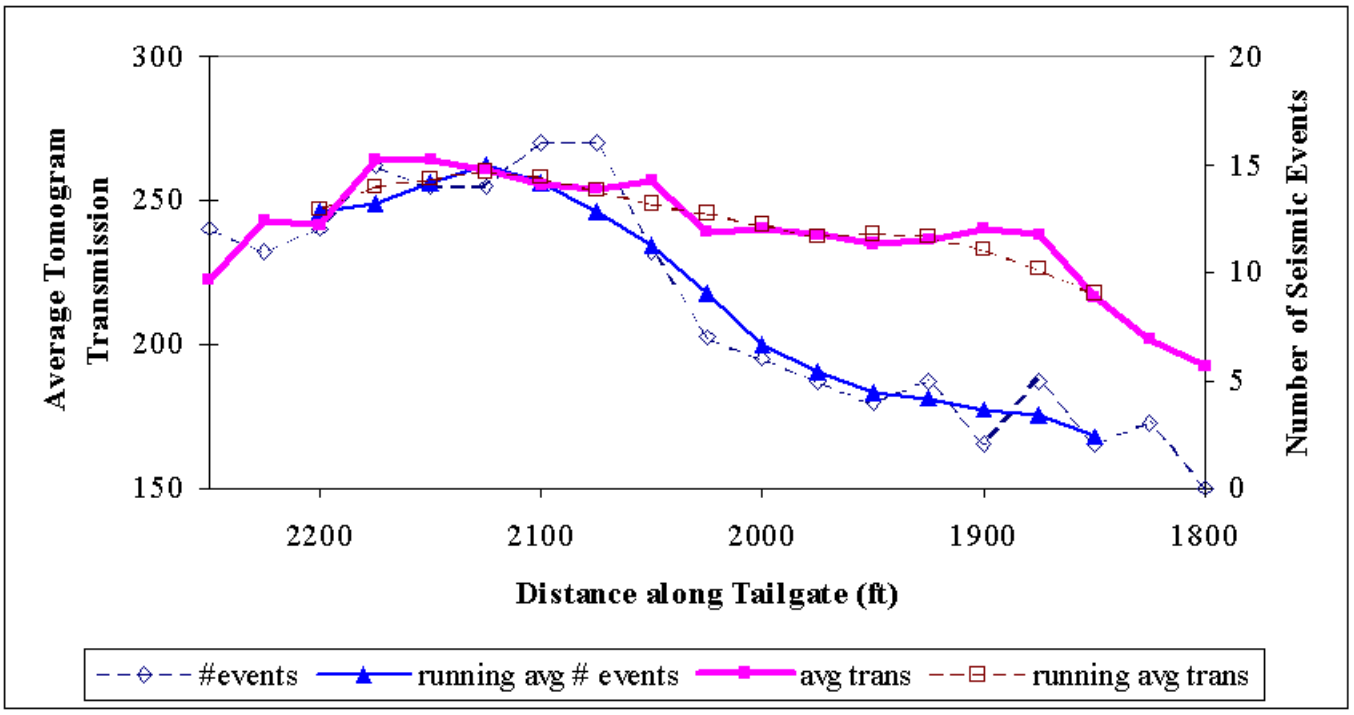


Figure 3. Number of seismic events and transmission measurement, average of all values across panel for locations along the tailgate

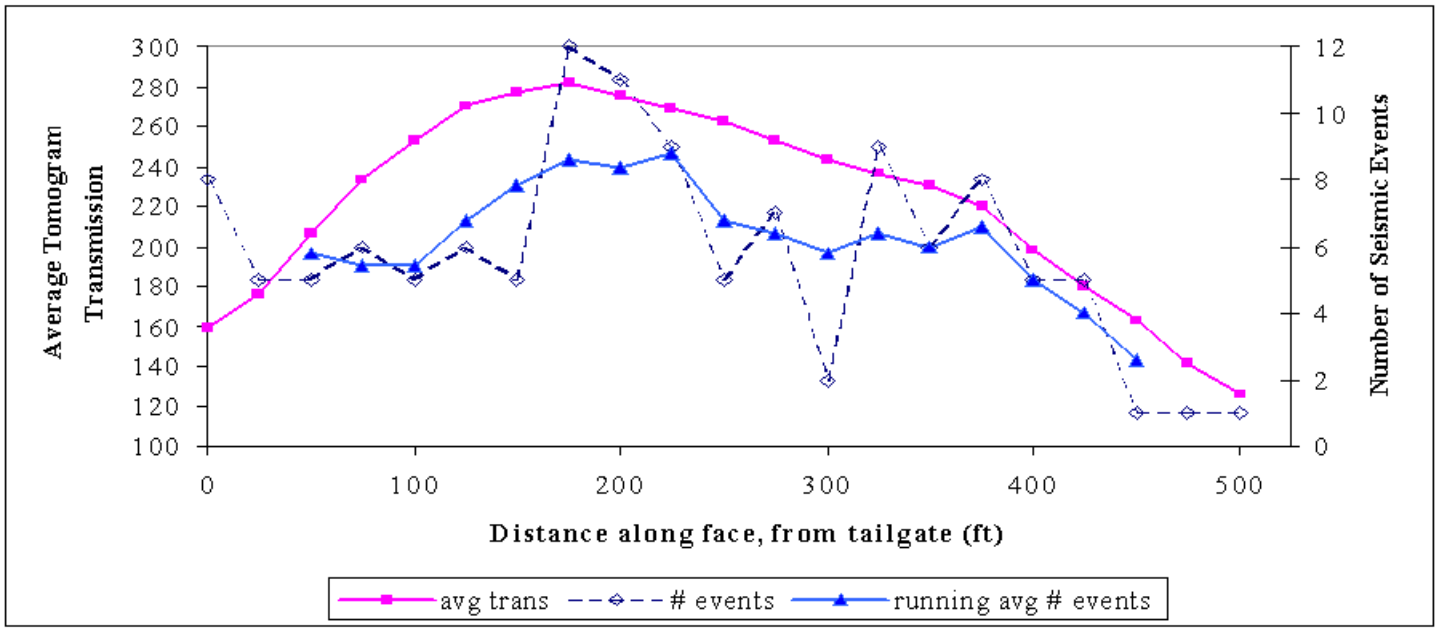


Figure 4. Number of seismic events and transmission measurement, average of all values along panel for locations along the face.

plotted against the number of seismic events occurring in the same strip and show that both increased seismic activity and higher tomography transmission values occur towards the beginning of the study period (Fig. 3). A good correlation is observed, and a correlation coefficient (R) of 0.77 was calculated. A similar calculation was done for locations across the face (in 7.5 m strips parallel to the face advance) with the results shown in Figure 4 and an R of 0.62.

To smooth the trends even more, a five-point running average of both of these calculations was determined and is also shown in Figures 3 and 4. An R of 0.94 was found for tailgate locations and an R of 0.89 was found for face locations using the running average trends. The high transmission (high stress) areas indicated by the tomograms correlate very well with the most seismically active areas indicated by the microseismic system. During this week, the high stress/high activity area was in the first days of the week and between shields 20 and 55.

*Six-Week Data Set*

Based on the good correlations found in analyzing the seismicity and tomography from the one week time period, another analysis using identical procedures was performed on a larger dataset spanning a six

week period. In addition to the seismicity and tomography, the shield-leg pressure data were also included in this larger analysis. The data for this analysis were collected as the face advanced from Station 2100 (February 17, 2000) to Station 1300 (March 30, 2000), a distance of 240 m. The results of this analysis are shown in the following figures: seismic events and event density are shown in Figure 5, the shield-leg pressure distribution is shown in Figure 6, and the average tomographic transmission is shown in Figure 7. Linear regression was used to correlate the data from the various source pairs and a coefficient of correlation was calculated. Plots of the correlations are as shown in Figures 8-10.

The strongest correlation was between shield-leg pressure and the average tomogram, which produced an R of 0.60 (Fig. 10). The correlation between seismicity and shield-leg pressures was 0.41, and that between seismicity and average tomogram was 0.20

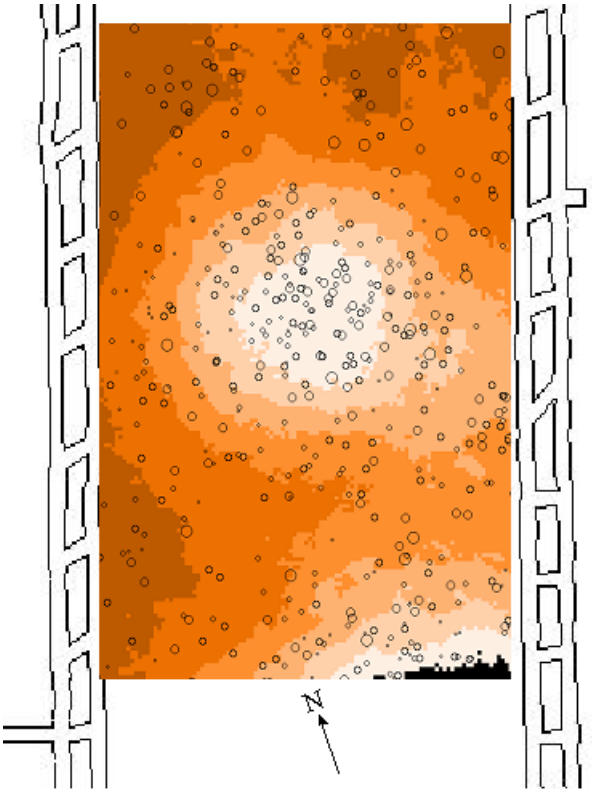


Figure 5. Seismic event location and density for six-week data set. Panel width is 160 m.

(Figs. 8, 9). When the data were smoothed by averaging strips parallel to the face as with the one-week data set, an R of only 0.33 was obtained. However, when averaging the data in strips perpendicular to the face an R of 0.92 was obtained.

## DISCUSSION AND CONCLUSIONS

The coefficient of correlation relating various results of the three monitoring systems ranges from 0.20 to 0.94. A potential explanation for the correlation is the influence on the three monitoring systems of the roof geology. Thicker, stronger sandstone layers in the

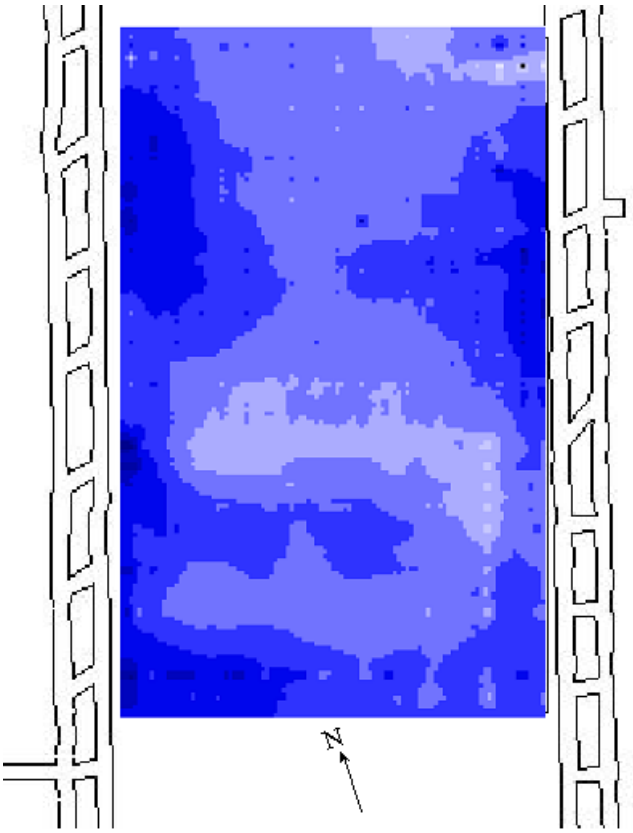


Figure 6. Shield-leg pressure distribution for six-week data set. Lighter areas indicated relatively higher loading than darker areas. Panel width is 160 m.

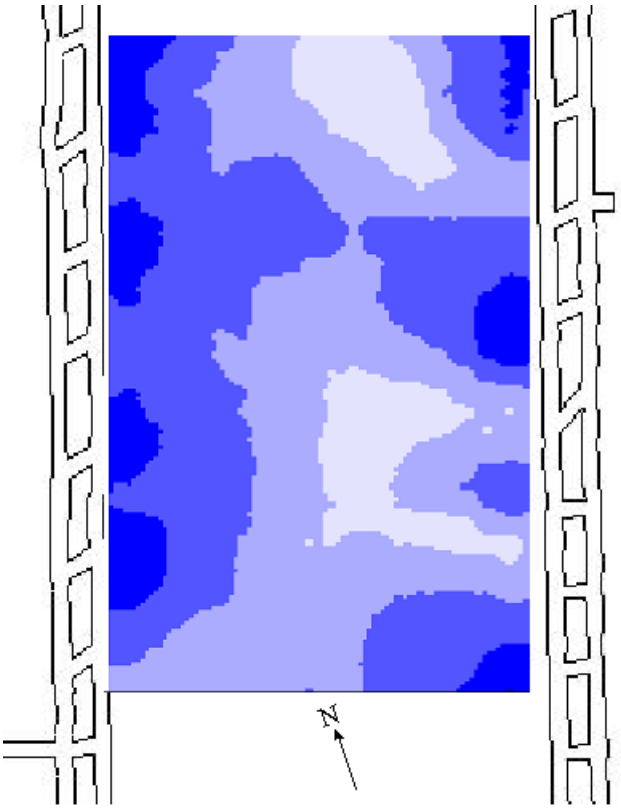


Figure 7 Average tomographic transmission for six-week data set. Lighter areas indicated relatively higher transmission than darker areas. Panel width is 160 m

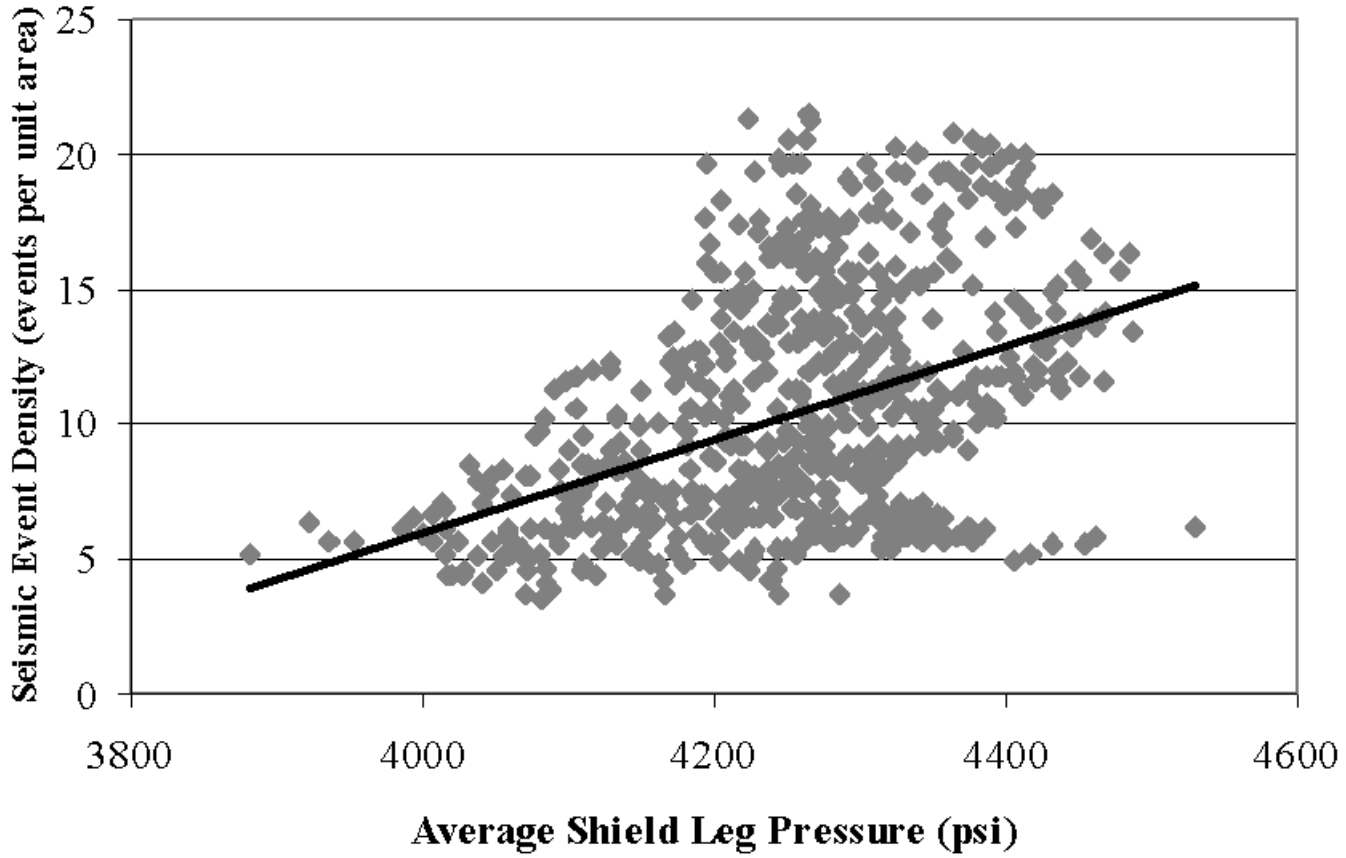


Figure 8. Correlation between seismic event density and average shield leg pressure for six-week data set.

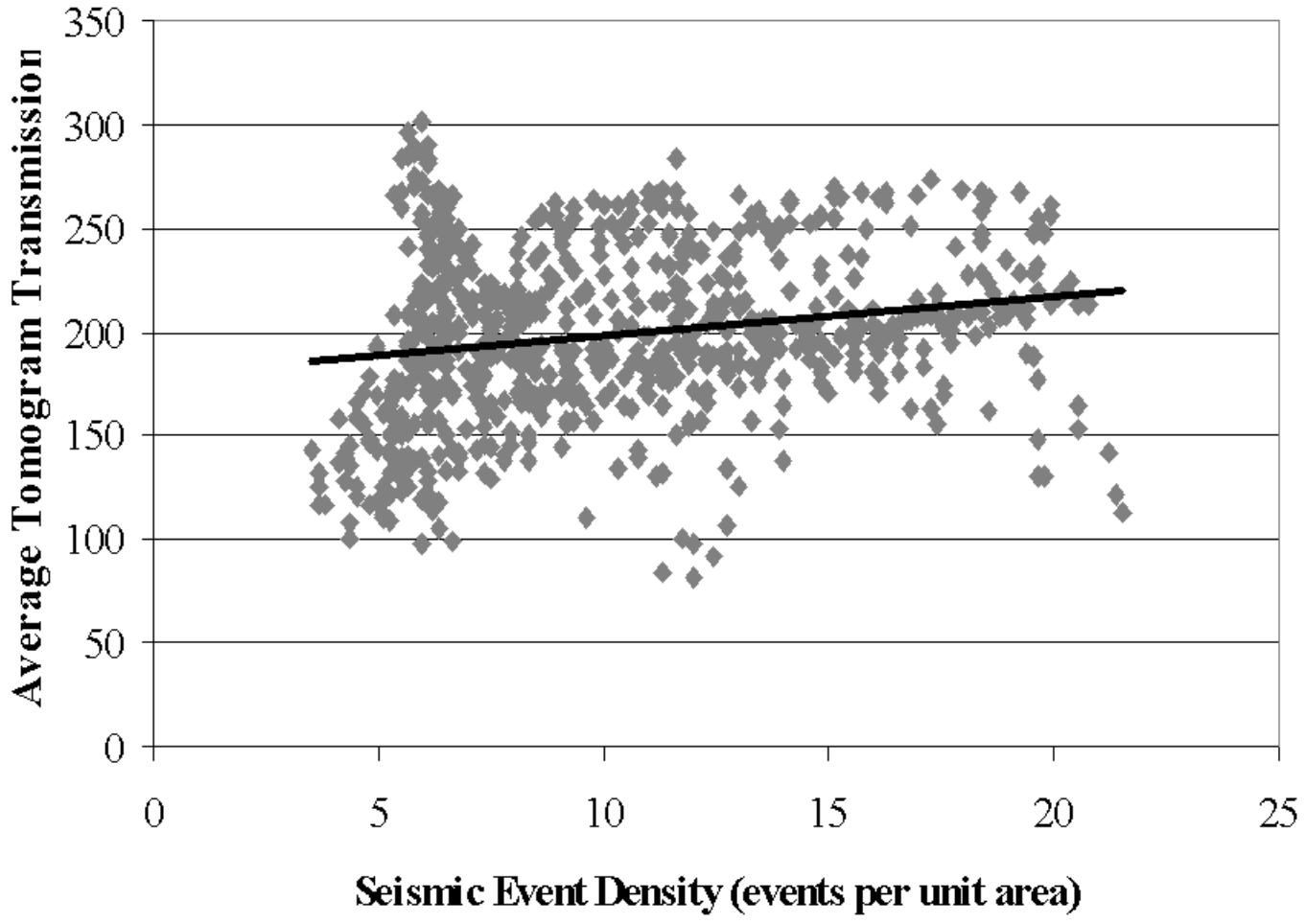


Figure 9. Correlation between seismic event density and average tomogram transmission for six-week data set.

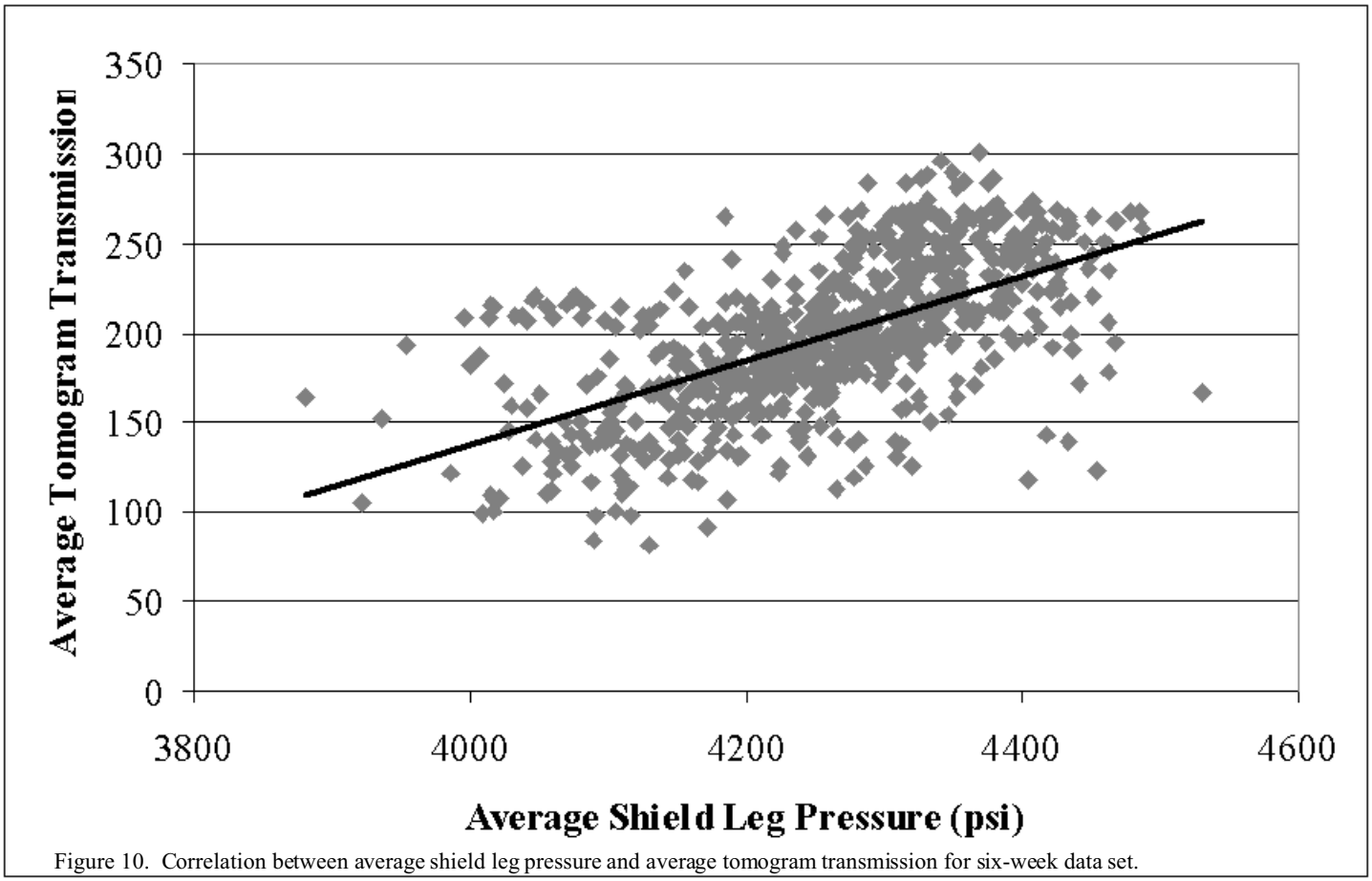


Figure 10. Correlation between average shield leg pressure and average tomogram transmission for six-week data set.

immediate roof appear on the tomograms as higher transmission levels than thinner, weaker beds. These thicker layers load the longwall shields more than thinner layers because the stronger layers tend to cantilever further over the shields before collapsing into the gob. Further, these more competent layers fail at higher stresses and generate more and/or larger seismic events in the abutment zone.

Regardless of the cause of the correlation, the fact that a correlation is observed is beneficial to the mining community. By implementing the tomography system, an indication of potential seismicity and shield-leg loading can be obtained for the region in advance of the mining face. If heavy loading or seismicity is projected, appropriate plans can be made, such as adjusting mining rates or minimizing personnel exposure until mining through the zone of concern is complete.

## REFERENCES


Arabasz, W.A., S.J. Nava & W.T. Phelps. 1997. Mining seismicity in the Wasatch Plateau and Book Cliffs coal mining districts, Utah, USA. In Gibowicz and Lasoki (eds), Rockbursts and Seismicity in Mines: 111-116. Rotterdam: Balkema.

Buchanan, D.J., R. Davis, P.J. Jackson & P.M. Taylor. 1981. Fault location by channel wave seismology in United Kingdom Coal Seams. Geophysics 46:994-1002.

Cormack, A.M. 1973. Reconstruction of densities from their projections, with applications in radiological physics. Phys. Med. Biol. 18(2): 195-207.

Cox, R.M., D.P. Conover & J.P. McDonnell. 1995. Integrated shield and pillar monitoring techniques for detecting catastrophic failures. In Proc. Mechanics and Mitigation of Violent Failure in Coal and Hard-Rock Mines. USBM Spec. Pub. 01-95: 119-140.

Dines, K.A. & J.R. Lytle. 1979. Computerized geophysical tomography. Proc. IEEE 67(7): 1065-1073.

Ellenberger, J.L., K.A. Heasley, P.L. Swanson & J. Mercier. 2001. Three dimensional microseismic monitoring of a Utah longwall. In Proc. 38th US Rock Mech. Symp. Washington, D.C., 7-10 July: in press. Rotterdam: Balkema.

Hanna, K., K.Y. Haramy & T.R. Ritzel. 1991. Automated longwall mining for improved health and safety at foidel creek mine. SME Preprint 91-165: 8pp.Haramy, K.Y. & J.P. McDonnell. 1988. Causes and control of coal mine bumps. USBM RI 9225: 35pp.

Holland, C.T. 1958. Cause and occurrence of coal mine bumps. In Trans. SME-AIME 211: 994-1004.

Hounsfield, G.N. 1973. Computerized transverse axial scanning (tomography). 1. description of system. Br. J. Radiol. 46(552): 1016-1022.

Iannacchione, A.T., A.A. Campoli & D.C. Oyler. 1987. Fundamental studies of coal mine bumps in the eastern united states. In Proc. 28th US Rock Mech. Symp.,

Tucson, June 29-July 1: 1063-1072. Rotterdam: Balkema.

Kormendi, A, L. Bodoky, L. Hermann, L. Dianisda & T. Kalman. 1986. Seismic measurements for safety in mines. Geophysical Prospecting 34: 1022-1037.

Kusznir, N.J. & I.W. Farmer. 1983. Rockburst phenomena in British coal mines. Rockbursts, Prediction and Control:103-115. London: IMM.

Mark, C., K.A. Heasley, A.T. Iannacchione & R.J. Tuchman. 1999. Proc. of the Second International Workshop on Coal Pillar Mechanics and Design. NIOSH IC 9448: 192 pp.

Mason, I.M. 1981. Algebraic reconstruction of a two-dimensional velocity inhomogeneity in the High Hazles Seam at Thoresby Colliery. Geophysics 46: 298-308.

Mendecki, A.J. 1997. Seismic Monitoring in Mines. London: Chapman and Hall.

Radon, J. 1917. Uber die bestimmung von functionen durch ihre integralwere lange gewisser mannigfaltigkeiten. Ber. Verh. Saechs. Akad. Wiss. 69: 262-267.

Swanson, P.L. 1995. Influence of mining-induced seismicity on potential for rock bursting. In Proc. Mechanics and Mitigation of Violent Failure in Coal and Hard-Rock Mines. USBM Spec. Pub. 01-95: 231-241.

Westman, E.C., K.Y. Haramy & A.D. Rock. 1996. Seismic tomography for longwall stress analysis. In M. Aubertin, F. Hassani & H. Mitri (eds) Proc. of 2nd North American Rock Mech. Symp., Montreal, 19-21 June: 397-403. Rotterdam: Balkema.

Wilson, P.E. & R.O. Kneisley. 1995. Mapping stress changes with microseismics for ground control during longwall mining. In Proc. Mechanics and Mitigation of Violent Failure in Coal and Hard-Rock Mines. USBM Spec. Pub. 01-95: 91-103.

Whittaker, B.N. 1983. Longwall planning with reference to rockbursts. Rockbursts, Prediction and Control: 117-122. London: IMM.

Young, R.P. 1992. Invited paper: correlation between seismic velocity and induced seismicity in underground mines. In J.R. Tillerson & W.R. Wawersik (eds) Proc. of 33rd US Rock Mech. Symp., Santa Fe, 3-5 June: 1113-1122. Rotterdam: Balkema.